ELSEVIER

Journal of Hazardous Materials 50 (1996) 183–198

JOURNAL OF HAZARDOUS MATERIALS

Blast characteristics and TNT equivalence values for some commercial explosives detonated at ground level

S.A. Formby *, R.K. Wharton

Health and Safety Laboratory, Health and Safety Executive, Harpur Hill, Buxton, Derbyshire, SK17 9JN, UK

Received 10 May 1995; accepted 4 March 1996

Abstract

We report measurement of the pressure–time profiles produced by the initiation at ground level of four common commercial sector explosives with different detonation velocities. The results indicate that there are no significant differences in the blast waveshapes from the explosives when measured at distances of 25 and 50 m from the initiation point. Analysis of both peak overpressure and positive phase impulse data has yielded values for the TNT Equivalence of the materials at two scaled distances. Our work indicates that the TNT Equivalence values of the materials studied vary with scaled distance and on whether they are evaluated from overpressure or impulse.

Keywords: Blast characteristic; TNT equivalence value; Commercial explosive; Ground-level detonation; Detonation velocity; Blast waveshape; Peak overpressure; Positive phase impulse data

1. Introduction

TNT Equivalence has been widely used to equate the blast effects produced by a given energetic material with those of the well characterised explosive TNT. In some cases the concept has been extended beyond explosives and applied to such events as dust explosions and vapour cloud explosions [1] where the analogy with TNT is less appropriate.

The Health and Safety Executive (HSE) is interested in evaluating TNT Equivalence, obtaining scaling laws and producing predictive techniques for both the near and far field blast effects from a range of explosives and energetic materials.

* Corresponding author.

PII S0304-3894(96)01791-8

A blast overpressure measurement facility has recently been constructed and commissioned at the Health and Safety Laboratory's site at Buxton to enable a detailed study to be undertaken in this area. While the blast range was being constructed, a contract was placed with British Gas plc to do a limited number of experiments at their Spadeadam test site. Surface mounted pressure transducers were used to monitor the pressures produced by the initiation at ground level of four commonly used commercial explosives. This paper presents our analysis and interpretation of the experimental data produced under this extra-mural contract.

2. Experimental

The explosives examined in this study were chosen to cover a range of ballistic mortar strengths and detonation velocities. Table 1 gives further details.

Hemispherical papier-mâché shells were used to contain the explosives. The hemispheres had a capacity of approximately 7 litres, a wall thickness of 2 mm, and an internal diameter of 340 mm. Each shell was coated internally and externally with varnish to provide a degree of waterproofing. Duplicate charges were prepared using each type of explosive: the mass of each set of charges differed because of the range of densities of the explosives.

Super Dopex was supplied in 12.5 kg blocks. Slices were carved from the explosive using a copper/beryllium knife and fitted into the container leaving as few air spaces as possible.

Special Gelatine 80 was supplied in 200 g cartridges. The gelatinous explosive was removed from the cartridges and pressed into the container, eliminating as much air as possible.

Penobel 2 was also supplied in 200 g cartridges. The powder explosive was removed from the cartridges and added to the container in increments, again eliminating as much air as possible.

Anobel was supplied as a free flowing powder which was poured into the container. As Anobel requires a booster to ensure detonation, each charge consisted of 6.5 kg Anobel with a 0.2 kg Special Gelatine 80 booster. Since the booster only accounted for 3% of the total mass of the charges, and the relative strengths of Special Gelatine 80 and Anobel are similar when determined by ballistic mortar measurements (Table 1), the effect of using a different explosive in the booster compared with the main charge was expected to be insignificant. We therefore analysed the resultant blast waves as though the charges consisted of 6.7 kg Anobel.

After filling each hemisphere with explosive, a membrane of transparent sealing film was stretched across the surface of the explosive and taped around the sides of the container.

On reaching the test site, charges were primed with a Nobel No. 8* detonator (and booster charge if necessary) located in the base of the charge prior to placing a plywood board 600 mm × 600 mm × 3 mm on top of the plastics film. The charge assembly was then inverted and placed on a bed of sand which was levelled prior to each test.

Some problems were experienced owing to flexibility of the hemispherical contain-

Table 1
Details of the explosives tested [a]

Explosive	Description	Uses	Velocity of detonation ($m s^{-1}$)	TNT Equivalence by ballistic mortar (%)	Density ($g cm^{-3}$)
Super Dopex	92–94% Nitro-Glycerine (NG) gelatinised with 6–8% nitrocellulose	Reference standard for ballistic mortar	7700 (Blasting Gelatine) [b]	98	1.6
Special Gelatine 80	NG based gelatinous explosive	General purpose excavation	3500	83	1.4
Anobel	Mixed, prilled ANFO blasting agent	Used generally in overburden blasting, opencast mining and quarrying operations	4000–5500 [c]	73	0.9
Penobel 2	NG powder permitted mining explosive (P4/5)	General purpose ripping and blasting operations in coal mines	2000	37	1.3

[a] All information was obtained from Ref. [2], unless otherwise indicated.
[b] Information from Ref. [3].
[c] Information from Ref. [4].

Table 2
Summary of tests

Test number	Explosive
1, 2	6.5 kg Anobel with 200 g Special Gelatine 80 booster
3, 4	7.8 kg Penobel 2
5, 6	9.6 kg Super Dopex
7, 8	9.5 kg Special Gelatine 80

ers: with Penobel 2 and Special Gelatine 80, cracks developed in the explosive during transportation of the charges.

With the exception of Anobel, it was necessary to apply pressure to the explosive to remove air pockets during charge manufacture. This produced distortion of the container and limited the amount of air that could be removed. On inversion of the Anobel charge, the sealing film was not rigid enough to prevent movement of the explosive, and a void at the top of the hemisphere may have been produced. It was not possible, therefore, to produce entirely homogeneous charges of uniform density, but we feel that any density variations will have been minor and will have therefore exerted little or no effect on the measurements.

Table 2 summarises the tests carried out.

The wind blew across the site from a S/SSW direction during the experiments, with a velocity in the range 3–9 $m\,s^{-1}$. Since the blast pressures were measured using piezo-electric gauges, rather than estimating them from the time of arrival of the blast waves, we believe that the effect of the wind on the blast wave parameters quoted in this paper will have been negligible.

3. Blast measurement details

Pressure measurements were made using ten Meclec MQ-10 piezo-electric gauges with a crystal resonance frequency of 80 kHz. Signals from these gauges were amplified and recorded on a Thorn–EMI Datatec BE256 transient recorder. The combined bandwidth of the amplifiers and filters used to condition the pressure signals was 20 kHz, and 12-bit samples were taken at a sampling rate of 50 or 80 kHz, depending on gauge location. The gauges had been dynamically calibrated to an accuracy of 1% on a separate calibration rig prior to the experiments.

Gauges were positioned flush with ground level at 25, 50, 75, 100 and 150 m from the firing position, as shown in Fig. 1. Gauges 1 to 4, 8 and 10 were in a horizontal line running approximately East–West at the same height as the firing point, while gauges 5, 6, 7 and 9 were all in a line at right angles, but at a lower level than the firing point. There were a number of earth embankments and cuttings around the test area, and the firing point was surrounded by such embankments.

The British Gas facility had been set up to measure overpressures from BLEVEs, with the explosions centred well above ground level. Although the gauges at the lower levels (5, 6, 7 and 9) are satisfactory for recording the overpressures from such events,

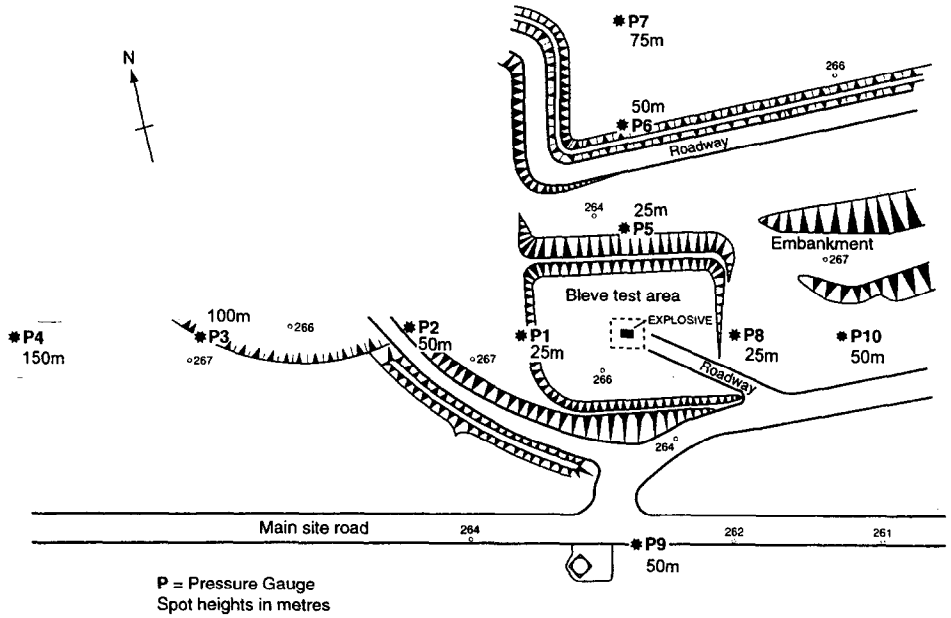

Fig. 1. Layout of the test site.

they would be expected to give low results for explosions at ground level. It is also expected that the presence of earth embankments around the initiation centre could have influenced the results recorded by the ground level gauges, as could reflections of the blast waves from obstacles around the test area.

The expected form of an ideal shock wave from an unconfined high explosive is shown in Fig. 2. It is characterised by an abrupt (essentially discontinuous) pressure increase at the shock front, followed by a quasi-exponential decay back to ambient

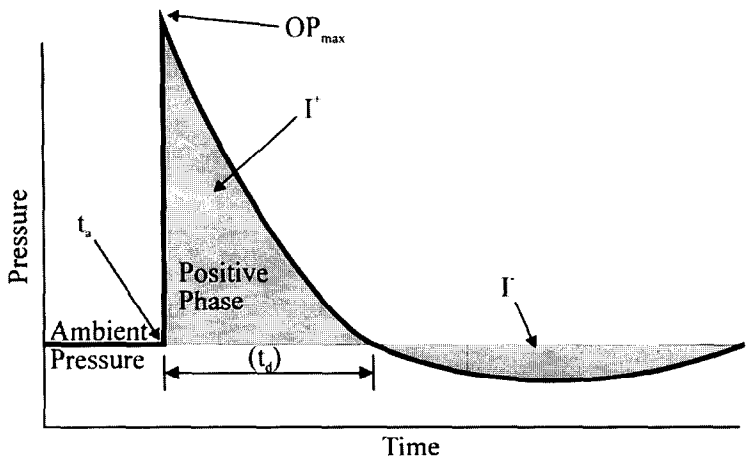

Fig. 2. Ideal shock wave in air.

pressure. A negative phase follows, in which the pressure is less than ambient, and oscillations between positive and negative overpressure continue as the disturbance quickly dies away. These further oscillations, being of low pressure difference, are not very important compared with the first positive phase, and usually are not examined.

The backslope of the positive phase of an ideal air blast wave is commonly fitted to the modified Friedlander equation, which is given [5] by $P'(t) = P_a + OP_{max}(1 - (t/t_d))e^{-bt/t_d}$ where b is a positive constant. The fitting of this equation to the upper portion of the backslope of a blast wave can be used to partially compensate for the non-ideal nature of pressure gauge recordings, caused by their finite response time and the presence of noise. This technique [6,7] was used to obtain the peak overpressures quoted in this paper.

It was found that many of the pressure–time recordings from the gauges at positions 3, 4, 5, 6, 9 and 10 did not exhibit the typical blast wave characteristics expected from condensed explosives. One example of a recording which appears to involve the superposition of different blast waves is given in Fig. 3. The non-ideal nature of certain of the pressure–time profiles is attributed to the topography of the site, since the pressure profiles recorded at gauges 1, 2 and 8, where there is a reduced likelihood of interference, were similar to the ideal shock waveshape. An example of a recorded blast wave which exhibits near ideal shock wave characteristics is shown in Fig. 4.

Comparison of Fig. 4 with the pressure profile from a non-typical blast wave, Fig. 5, indicates that the rate of increase of pressure in the non-typical blast wavefront is lower than in a shock wave. The gradient of the shock front is critical to the energy dissipation within the wave as it travels through the air, since this is the region in which non-isentropic compression occurs [8]. In order to provide a meaningful comparison between the measured blast waves from commercial sector explosives and those

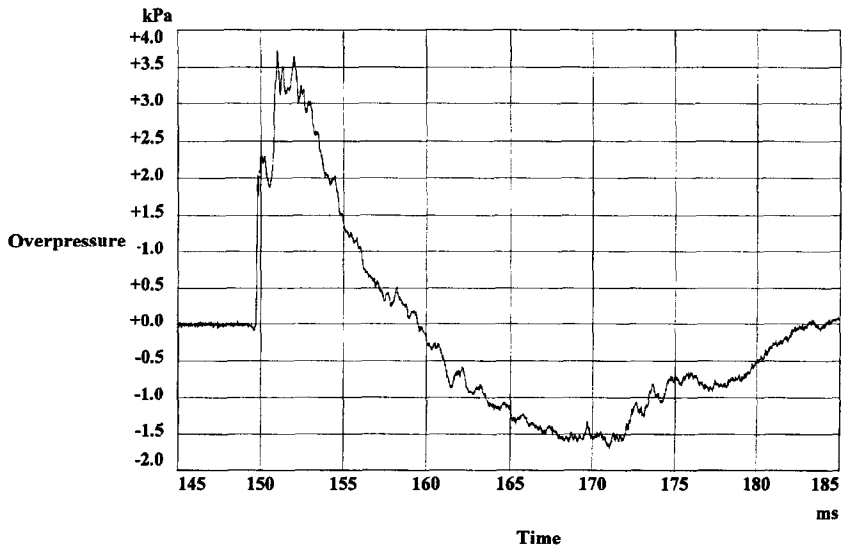

Fig. 3. Example of a recording showing superposition of blast waves.

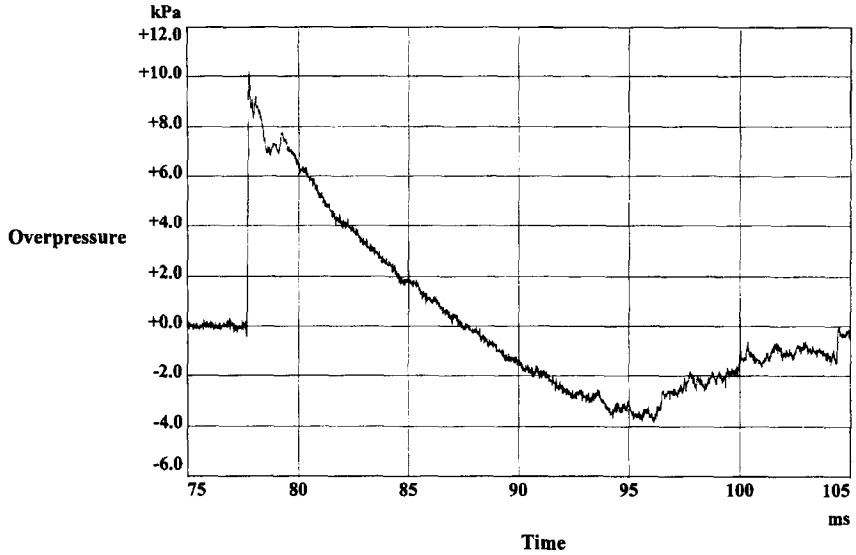

Fig. 4. Example of a recording exhibiting shock wave characteristics.

published for TNT, only pressure waves which exhibited near ideal waveshapes were analysed to obtain values for OP_{max} and I^+, see Table 3.

Some of the pressure gauge signals were found to be degraded by the presence of noise. Eliminating this interference by conventional moving-window averaging techniques was not considered an appropriate method for improving the quality of the data,

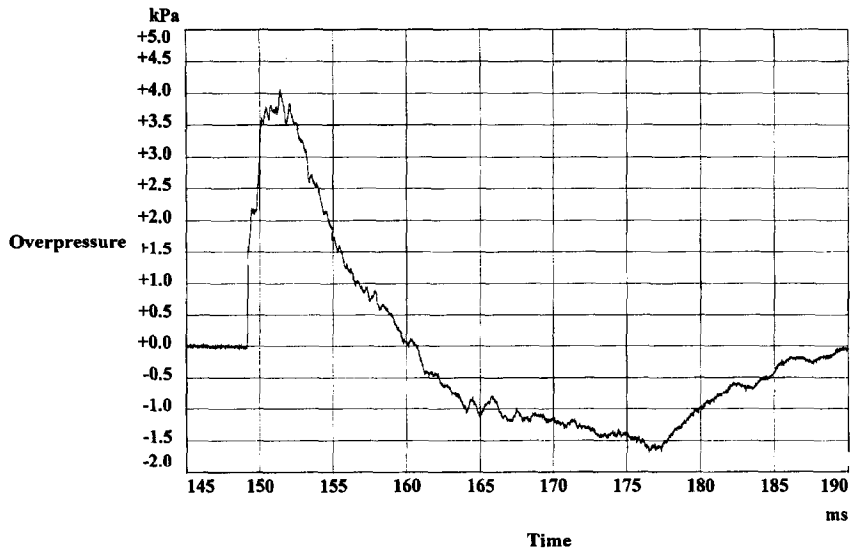

Fig. 5. Example of a recording exhibiting non-ideal blast wave characteristics.

Table 3
Recordings analysed for blast wave characteristics

Test number	Gauge recordings used
1	P1, P2, P8
2	P1, P8
3	P1, P2, P8
4	P1, P2, P8
5	P1, P2, P5, P8, P9
6	P1, P2, P5, P8
7	P1, P2, P8, P9
8	P1, P2, P8, P9

since this would have seriously reduced the value of OP_{max}. The signals were therefore digitally post-filtered, removing those frequencies that were consistent with noise. We estimate that this caused an average reduction in OP_{max} of only 1–2%.

4. Measurement of shockwave characteristics

The values for OP_{max} and I^+ for those pressure recordings that exhibited shock wave behaviour were calculated and then scaled to mean sea-level conditions and 1 kg of material, using Sachs' relationships [9]:

$$Z = \frac{R}{W^{\frac{1}{3}}\left(\frac{P_0}{P_a}\right)^{\frac{1}{3}}} \tag{1}$$

$$P = \frac{P'}{\left(\frac{P_a}{P_0}\right)} \tag{2}$$

$$\zeta^+ = \frac{I^+}{W^{\frac{1}{3}}\left(\frac{P_0}{P_a}\right)^{\frac{2}{3}}\left(\frac{T_0}{T_a}\right)^{\frac{1}{2}}} \tag{3}$$

$$\tau = \frac{t}{W^{\frac{1}{3}}\left(\frac{P_a}{P_0}\right)^{\frac{1}{3}}\left(\frac{T_0}{T_a}\right)^{\frac{1}{2}}} \tag{4}$$

Ambient temperature and pressure measurements were provided by the Meterological Office weather station at Carlisle, and adjusted to take account of the altitude of the test site (approximately 270 m). The average ambient air pressure and temperature during tests 1 to 3 were 97 500 Pa and 278 K, respectively. Tests 4 to 8 were conducted with an

Table 4
Summary of data evaluated from the tests

Test number	Gauge	Charge mass (kg)	Distance to gauge (m)	Z ($m\,kg^{-1/3}$)	OP_{max} (Pa)	OP_{max} error (Pa)	I^+ (Pa s)	I^+ error (Pa s)	ζ^+ (Pa s $kg^{-1/3}$)	ζ^+ error (Pa s $kg^{-1/3}$)	t_a (ms)	τ_a (ms $kg^{-1/3}$)	t_d (ms)	τ_d (ms $kg^{-1/3}$)
1	P1	6.7	25	13.2	7522	218	21.4	0.2	11.0	0.1	85.2	44.8	7.8	4.1
1	P2	6.7	50	26.3	3466	215	13.8	0.2	7.1	0.1	157.5	82.8	9.0	4.7
1	P8	6.7	25	13.2	6505	268	16.3	0.2	8.4	0.1	79.3	41.7	6.9	3.6
2	P1	6.7	25	13.2	6177	293	20.4	0.2	10.5	0.1	83.9	44.1	8.1	4.3
2	P8	6.7	25	13.2	6137	287	16.0	0.2	8.2	0.1	80.5	42.3	6.6	3.5
3	P1	7.8	25	12.5	3807	272	10.3	0.1	5.0	0.1	87.5	43.7	6.1	3.0
3	P2	7.8	50	25.0	1881	128	5.9	0.1	2.9	0.1	160.5	80.2	6.9	3.4
3	P8	7.8	25	12.5	3947	269	7.8	0.1	3.8	0.1	86.8	43.4	5.4	2.7
4	P1	7.8	25	12.5	3850	179	10.4	0.1	5.1	0.1	87.3	44.1	6.1	3.1
4	P2	7.8	50	25.0	1812	176	5.8	0.1	2.8	0.1	160.2	81.0	6.9	3.5
4	P8	7.8	25	12.5	4315	245	8.0	0.1	3.9	0.1	84.0	42.5	5.5	2.8
5	P1	9.6	25	11.6	12180	377	50.7	0.5	23.2	0.2	76.9	36.3	10.4	4.9
5	P2	9.6	50	23.3	5242	205	26.7	0.3	12.2	0.1	148.1	69.9	12.0	5.7
5	P5	9.6	25	11.6	14439	349	36.9	0.4	16.9	0.2	84.5	39.9	9.0	4.2
5	P8	9.6	25	11.6	11750	314	32.4	0.3	14.8	0.1	77.3	36.5	8.5	4.0
5	P9	9.6	50	23.3	4086	160	22.2	0.2	10.1	0.1	153.5	72.4	12.8	6.0
6	P1	9.6	25	11.6	10869	411	48.6	0.5	22.2	0.2	78.0	36.8	10.6	5.0
6	P2	9.6	50	23.3	5366	234	26.3	0.3	12.0	0.1	149.8	70.7	12.4	5.9
6	P5	9.6	25	11.6	13812	465	37.7	0.4	17.2	0.2	85.7	40.4	8.9	4.2
6	P8	9.6	25	11.6	11209	315	33.1	0.3	15.1	0.1	77.5	36.6	8.4	4.0
7	P1	9.5	25	11.7	9704	403	39.0	0.4	17.9	0.2	77.7	36.8	9.9	4.7
7	P2	9.5	50	23.4	4428	303	21.8	0.2	10.0	0.1	149.7	70.9	11.6	5.5
7	P8	9.5	25	11.7	10198	306	24.7	0.3	11.3	0.1	77.8	36.8	6.9	3.3
7	P9	9.5	50	23.4	3593	324	16.8	0.2	7.7	0.1	154.4	73.1	11.6	5.5
8	P1	9.5	25	11.7	10076	408	39.2	0.4	18.0	0.2	79.1	37.4	9.8	4.6
8	P2	9.5	50	23.4	4127	252	21.8	0.2	10.0	0.1	151.3	71.6	11.5	5.4
8	P8	9.5	25	11.7	9893	319	25.6	0.3	11.7	0.1	79.6	37.7	7.2	3.4
8	P9	9.5	50	23.4	3503	533	16.8	0.3	7.7	0.1	155.1	73.4	11.9	5.6

average ambient air pressure of 96 800 Pa and air temperature of 283 K. The Sachs-scaled results are summarised in Table 4.

The method used to estimate OP_{max} was that previously reported by Kinney and Graham [6], and Ismail and Murray [7]. If t in the modified Friedlander equation is measured from the time of arrival of the blast wave, then when t is small, $(1 - t/t_d) \rightarrow 1$, so $d\ln(P - P_a)/dt \rightarrow -\frac{b}{t_d}$. Hence the natural logarithm of the overpressure $(P - P_a)$ in a blast wave, plotted against time, should be a straight line after OP_{max}. Extrapolation to time = 0 will yield $\ln(OP_{max})$, and provide an estimate of OP_{max} at the arrival time of the blast wave. Peak overpressure values calculated by this method were then Sachs-scaled to mean sea level conditions.

The specific procedure used to analyse the results reported in this paper was to:

1. Plot ln(overpressure) against time.
2. Fit a straight line to the top portion (15%) of the backslope, after the recorded peak.
3. Extrapolate this line back to t_a.
4. Find the value of $\ln(OP_{max})$.
5. Sachs-scale OP_{max} to mean sea-level conditions.

Fig. 6 shows peak overpressure against scaled distance for the explosions initiated in these trials. The uncertainty in the data points is mainly due to variations between the two repeat experiments on each material, and is between 5 and 15%.

The positive phase impulse (per unit area) is given by $I^+ = \int_{t_a}^{t_d} P(t)dt$, and was calculated by numerical integration of the recorded blast waves using FAMOS software [10]. Impulse values calculated by this method were then Sachs-scaled to mean sea level conditions and 1 kg of material. Fig. 7 illustrates the dependence of scaled impulse on

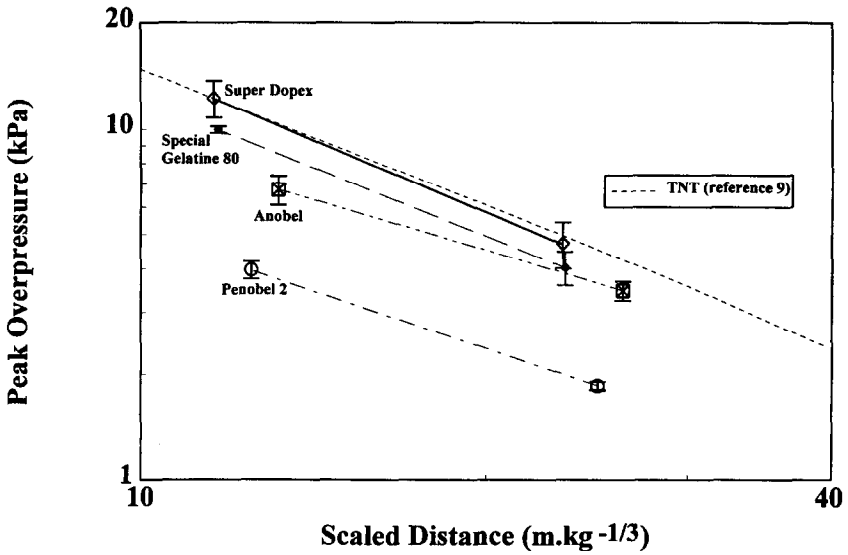

Fig. 6. The dependence of peak overpressure on scaled distance.

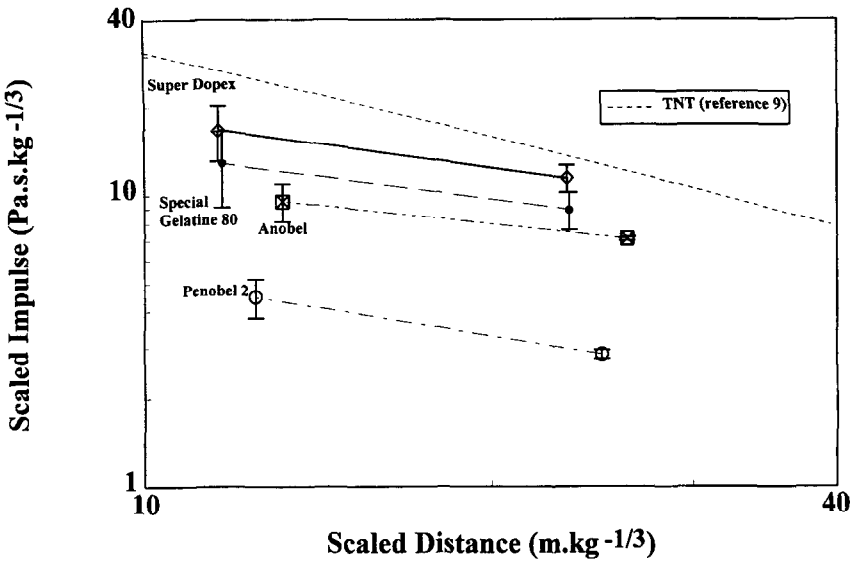

Fig. 7. The dependence of scaled impulse on scaled distance.

scaled distance for the explosives examined in this study. The uncertainty in the data points is again mainly due to variations between the two repeat experiments on each material, and was a maximum of 29% (for Special Gelatine 80).

5. Calculation of TNT equivalence

The TNT Equivalence (TNT_e) of a material is given [11] by:

$$TNT_e(\%) = 100 \times \left(\frac{W_{TNT}}{W_x} \right)_{OP_{max}, I^+} \tag{5}$$

where W_x = mass of explosive charge and W_{TNT} = mass of TNT producing the same peak overpressure, or positive impulse, at the same distance.

This was calculated for the recorded blast waves using the methods described by Maserjian and Fisher [12], and published TNT hemispherical groundburst data [9]. These methods for calculation of TNT Equivalence have also previously been used by Esparza [13]. TNT Equivalence by overpressure can be calculated from the following relationship:

$$[TNT_e]_{OP_{max}} = \left(\frac{Z_x}{Z_{TNT}} \right)^3_{OP_{max}} \tag{6}$$

where Z_x = scaled distance from the explosive charge and Z_{TNT} = scaled distance from TNT producing the same OP_{max}.

Since an OP_{max} of 1857 Pa was recorded from Penobel 2 at $Z = 25.0$, and the lowest TNT pressure reported in Ref. [9] is 2360 Pa at $Z = 40$, it was necessary to extrapolate

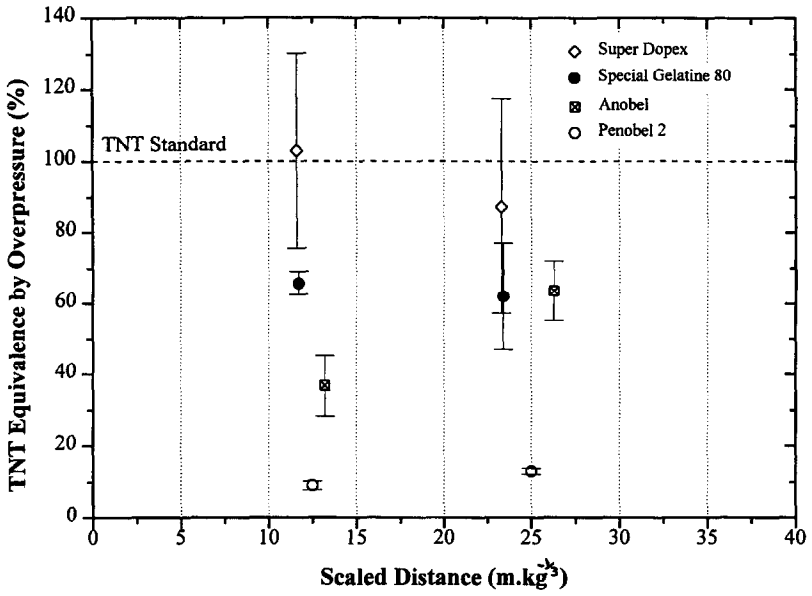

Fig. 8. The dependence of $[TNT_e]_{OP_{max}}$ on scaled distance.

the published data to $Z = 50$ in order to evaluate $[TNT_e]_{OP_{max}}$. A straight line was fitted to the low pressure TNT data points on a log–log graph against Z. This yielded a gradient of -1.30 which is in reasonable agreement with the value of -1.38 reported

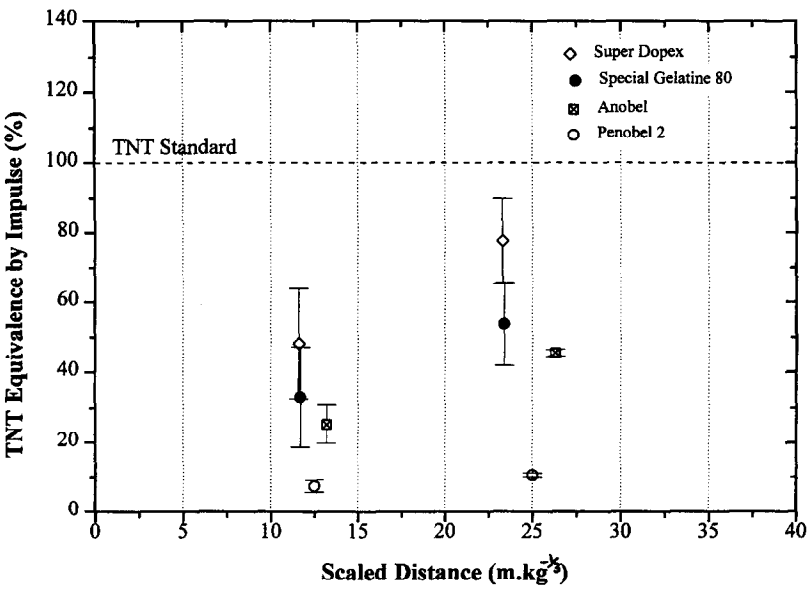

Fig. 9. The dependence of $[TNT_e]_{I^+}$ on scaled distance.

by Honma et al. [14] for a range of weak (< 200 Pa) shocks in air. Since the line drawn was a satisfactory fit to the published low pressure data, the value of −1.30 was used in all subsequent calculations. Fig. 8 illustrates the dependence on scaled distance of TNT Equivalence evaluated in this manner.

In order to obtain the TNT Equivalence by impulse, $[TNT_e]_{I^+}$, using the method of Maserjian and Fisher [12] it was necessary to obtain the intersection point of a construction line of unity gradient with the TNT impulse curve, yielded by a plot of ζ^+ against Z. In order to simplify calculation of the intersection point, it was found that published TNT impulse data for groundburst [9] when plotted on a log–log graph against Z could be adequately approximated by a straight line dependence in the region of interest.

A scaled impulse of 2.85 s Pa kg$^{-1/3}$ was recorded from Penobel 2 at $Z = 25.0$, and the lowest TNT scaled impulse reported in Ref. [9] is 7.92 s Pa kg$^{-1/3}$ at $Z = 40$. It was therefore necessary to extrapolate the published TNT impulse data in a similar manner to that described for OP_{max} above, in order to evaluate $[TNT_e]_{I^+}$ for Penobel 2 at $Z = 25.0$. The published data for scaled impulse was extrapolated to $Z = 53$, using a straight line of gradient −1.0 fitted to the low impulse data points on a log–log graph against Z. Fig. 9 illustrates the dependence of TNT Equivalence calculated by impulse on scaled distance for the experiments reported in Table 4.

6. Comparison of TNT equivalence from overpressure and impulse

Figs. 8 and 9 indicate that different values of TNT Equivalence are obtained from overpressure and impulse data. In order to investigate the relative magnitude of the two

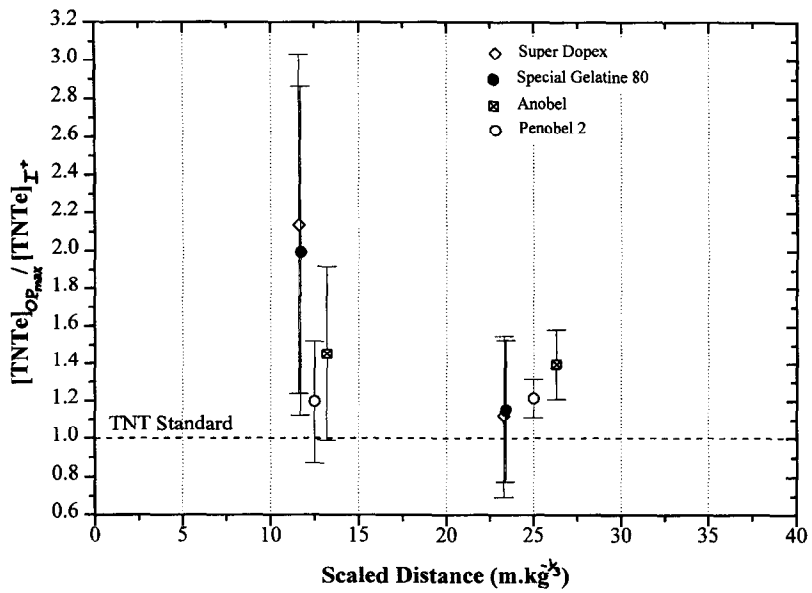

Fig. 10. The dependence of $[TNT_e]_{OP_{max}}/[TNT_e]_{I^+}$ on scaled distance.

values, the ratio ($[TNT_e]_{OP_{max}}/[TNT_e]_{I^+}$) was calculated for each experiment and the values plotted against Z, Fig. 10. Although only limited data are available and the error bars on the graph are large, it can be concluded that, generally, $[TNT_e]_{OP_{max}} > [TNT_e]_{I^+}$.

7. Discussion and conclusions

At the sensor locations used for these tests, there was no significant difference in blast waveshape from explosives with different detonation velocities. It had been expected that blast waves from explosives with slower energy release rates would have taken longer to ramp up into shock waves. The fact that this was not observed is attributed to the large distances between the charge and gauges.

The topography of the site affected many of the pressure recordings, as embankments and other obstacles interfered with blast wave propagation. It is expected that the propagating blast waves would have been affected to differing degrees by both diffraction (as they travel over surrounding embankments) and by reflection (from obstacles around the test area). Many of the recordings of blast waves that had suffered interference exhibited non-shock wave characteristics, and pressure recordings affected in this way were not used in the evaluation of TNT Equivalence. Signal traces from locations 1, 2 and 8 were found to possess characteristics similar to those of an ideal shock wave, because the blast waves at these positions had travelled over smoother terrain than that used for the location of the other gauges on the site. These recordings were used to evaluate TNT Equivalence for the explosives studied. Ideally, in order to make measurements which can be used to compare blast waves from explosive sources with those reported for TNT, a flat area of land is needed which is free from obstructions that could interfere with the blast waves.

TNT Equivalences obtained from this study are summarised in Table 5. The values given for the explosive Anobel should only be considered as rough estimates, since it has been reported [4] that an unconfined charge size of at least 450 kg is needed before ANFO can be considered to release its full energy. Free-field blast measurements with ANFO [4] have yielded TNT Equivalence values of about 85%.

The significant difference between the TNT Equivalence values calculated from our data for Penobel 2, and the value obtained from ballistic mortar measurements [2], Table

Table 5
TNT Equivalence values of some commercial explosives

Explosive	$[TNT_e]$ by ballistic mortar (%)	$[TNT_e]_{OP_{max}}$ (%)		$[TNT_e]_{I^+}$ (%)	
		Scaled distance ($m\,kg^{-1/3}$)		Scaled distance ($m\,kg^{-1/3}$)	
		13	25	13	25
Super Dopex	98	103	87	48	77
Special Gelatine 80	83	66	62	33	54
Anobel	73	37 [a]	64 [a]	25 [a]	46 [a]
Penobel 2	37	9 [a]	13 [a]	8 [a]	11 [a]

[a] For indication only, as it is likely that these materials did not fully detonate in the tests reported here.

5, may be due to the lower confinement of the material in the airblast trials. Penobel 2 is a permitted mining explosive which is designed to release its full energy only when confined.

Since the experiments used a groundburst configuration, the hardness of the ground is an additional variable that could have affected the TNT Equivalences evaluated in this paper. The proportion of explosion energy radiated as a blast wave will depend upon the energy absorbed during crater formation, and the absorption coefficient of the ground. Although the absorption coefficient is not known, comparing the blast gauge recordings with published hemispherical groundburst, rather than airburst, TNT data ensures that, as far as possible, the most accurate TNT Equivalences have been evaluated from our data.

Although this paper presents only limited information from some initial studies on blast, it is still possible to draw two general conclusions from our work: the TNT Equivalences for the materials studied are different depending on whether they are evaluated using overpressure or impulse data; and the values of TNT_e evaluated from overpressure are generally greater than those evaluated from impulse.

Other authors have previously reported that the TNT Equivalence of certain explosives is distance-dependent. For example, De Yong and Campanella [15] have published information indicating that the TNT Equivalences calculated by overpressure for a range of primary explosives and pyrotechnics vary with distance. Swisdak has also reported that the TNT Equivalence of some high explosives (e.g. Composition B, Composition C-4, Pentolite, and Tritonal) varies with distance and with the method of calculation [16].

The programme of air burst experiments with commercial sector energetic materials that is currently under way using the new facility at Buxton will generate much useful information. The results obtained from these studies will enable a detailed examination to be made of both the applicability of TNT Equivalence to quantification of the airblast hazard from a range of detonating materials, and the general applicability of the above observations.

8. Nomenclature

The following symbols are used in this paper:

W	charge mass (kg)
R	distance (m)
t	time (s)
t_a	arrival time of blast wave (s)
t_d	positive phase duration (s)
$P'(t)$	pressure at time t (Pa)
$P(t)$	Sachs' scaled pressure at time t (Pa)
P_a	ambient atmospheric pressure (Pa)
P_0	standard atmospheric pressure (101 300 Pa)
OP_{max}	peak overpressure (Pa)
T_a	ambient air temperature (K)

T_0	standard air temperature (288 K)
I	impulse (Pa s)
I^+	positive phase impulse (Pa s)
I^-	negative phase impulse (Pa s)
Z	scaled distance ($m\,kg^{-1/3}$)
τ	scaled time ($s\,kg^{-1/3}$)
ζ^+	scaled positive phase impulse ($Pa\,s\,kg^{-1/3}$)
TNT_e	TNT Equivalence (%)
$[TNT_e]_{OP_{max}}$	TNT Equivalence derived from overpressure data (%)
$[TNT_e]_{I^+}$	TNT Equivalence derived from positive phase impulse data (%)

Acknowledgements

The authors are grateful to Mr A.J. Barratt (HSE) for undertaking the experimental work with the assistance of members of staff from the British Gas site at Spadeadam, and to Mr A.E. Jeffcock (HSE) for assisting with preliminary data analysis.

References

[1] C. Sadee, D.E. Samuels and T.P. O'Brien, The characteristics of the explosion of cyclohexane at the Nypro (UK) Flixborough Plant on 1st June 1974, J. Occup. Accid., 1(3) (1976) 203–235.
[2] J. Köhler and R. Meyer, Explosives, VCH, Weinheim, 4th edn., 1993.
[3] A. Marshall, Explosives, Vol. 2: Properties and Tests, 2nd edn., J.A. Churchill, London, 1917, p. 491.
[4] J. Petes and K. Tempo, ANFO Detonation and Blast Characteristics of 600 ton Unconfined Charges, Proc. 12th Int. Symp. Explosives and Pyrotechnics, 1984, 1/99–110.
[5] W.E. Baker, Explosions in Air, University of Texas Press, 1973, pp. 5, 57 and 64.
[6] G.F. Kinney and K.J. Graham, Explosive Shocks in Air, 2nd edn., Springer, 1962, pp. 100–102.
[7] M.M. Ismail and S.G. Murray, Study of the blast wave parameters from small scale explosions, Propellants, Explosives, Pyrotechnics 18 (1993) 11–17.
[8] R.H. Cole, Underwater Explosions, Princeton University Press, New Jersey, USA, 1948, p. 18.
[9] C.N. Kingery and G. Bulmash, Airblast Parameters from TNT Spherical Air Burst and Hemispherical Surface Burst, ARBRL-TR-02555, US Army Armament Research and Development Center, BRL, Aberdeen Proving Ground, Maryland, USA, 1984.
[10] FAMOS (Fast Analysis and Monitoring Of Signals) User's Manual, imc Mess-systeme GmbH, Berlin, Germany, 1993.
[11] M. Held, TNT-Equivalent, Propellants, Explosives, Pyrotechnics, 8 (1983) 158–167.
[12] J. Maserjian and E.M. Fisher, Determination of Average Equivalent Weight and Average Equivalent Volume and their Precision Indices for Comparison of Explosives in Air, NAVORD Report 2264, US Naval Ordnance Laboratory, White Oak, Maryland, USA, 1951.
[13] E.D. Esparza, Blast measurements and equivalency for spherical charges at small scaled distances, Int. J. Impact Eng., 4(1) (1986) 23–40.
[14] H. Honma, I.I. Glass, C.H. Wong, O. Holst-Jensen and D.Q. Xu, Experimental and numerical studies of weak blast waves in air, Shock Waves, 1 (1991) 111–119.
[15] L.V. De Yong and G. Campanella, A study of blast characteristics of several primary explosives and pyrotechnic compositions, J. Hazard. Mater., 21 (1989) 125–133.
[16] M.M. Swisdak, Jr., Explosion Effects and Properties, Part 1: Explosion Effects in Air, NSWC/WOL/TR 75-116, Naval Surface Weapons Center, White Oak, USA, 1975.